Supporting information for

Enhanced surface reaction kinetics and charge separation of p-n heterojunction Co_3O_4/$BiVO_4$ photoanodes

Xiaoxia Chang, Tuo Wang, Peng Zhang, Jijie Zhang, Ang Li and Jinlong Gong*

Key Laboratory for Green Chemical Technology of Ministry of Education, School of Chemical Engineering and Technology, Tianjin University; Collaborative Innovation Center of Chemical Science and Engineering, Tianjin 300072, China

* Corresponding author: jlgong@tju.edu.cn; Fax: +86-22-87401818

Contents

Experimental section

Materials

Bismuth nitrate pentahydrate ($Bi(NO_3)_3 \cdot 5H_2O$, > 99.0%) was purchased from Tianjin FuChen Chemical Factory. Vanadyl acetylacetonate ($VO(acac)_2$, 98%) and *p*-benzoquinone (≥ 98.0%) were supplied by *J&K* Scientific Ltd. Potassium iodide (KI, ≥ 95%), acetone (GR), ethanol (GR), nitric acid (HNO_3, 26-28 wt%), ammonium solution ($NH_3 \cdot H_2O$, 25 wt%), cobalt acetate ($C_4H_6O_4 \cdot Co \cdot 4H_2O$, ≥ 97%) and dimethyl sulfoxide (DMSO, 99.5%) were purchased from Tianjin GuangFu Fine Chemical Research Institute. High purity water (18.25 MΩ·cm) supplied by a UP Water Purification System was used in the whole experimental processes. All the reagents were used without any purification process. FTO substrates ($F:SnO_2$, 14 Ω per square) were purchased from Nippon Sheet Glass, Japan. And before using, the FTO substrates were ultrasonically cleaned for 20 min each in deionized water, ethanol, and acetone, respectively.

Preparation of $BiVO_4$ electrodes

Synthesis of nanoporous $BiVO_4$ films on FTO substrates involves two steps—electrodeposition of BiOI films on FTO substrates and synthesis of the nanoporous $BiVO_4$ films. The electrodeposition of BiOI films by the reduction of *p*-benzoquinone to hydroquinone has been described previously.[1] Briefly, 20 mmol KI was dissolved into 50 mL deionized water and stirred for 15 min, then its pH was adjusted to 1.7 by adding HNO_3. After stirring for another 15 min, 2 mmol $Bi(NO_3)_3 \cdot 5H_2O$ was added to the solution and then the mixture was stirred for another 15 min to form the plating solution. This solution was mixed with 20 mL of absolute ethanol containing 4.6 mmol *p*-benzoquinone, and was vigorously stirred for a few minutes. Electrodeposition in the prepared electrolytic bath was carried out potentiostatically in a typical three-electrode system using a FTO substrate (3 × 1 cm^2) as the working electrode (WE), a platinum foil (2 × 2 cm^2) as the counter electrode (CE) and saturated Ag/AgCl as the reference electrode (RE). As an optimized condition, electrodeposition was conducted at -0.1 V *vs.* Ag/AgCl for 5 min.[2] Afterwards, the FTO substrate was rinsed with deionized water and dried in ambient air.

$BiVO_4$ electrodes were prepared by placing 0.2 mL of a dimethyl sulfoxide (DMSO) solution containing 0.2 M vanadyl acetylacetonate ($VO(acac)_2$) on the BiOI electrodes, followed by heating in a muffle furnace at 450 ºC (ramping rate 1 ºC/min) for 2 h. After cooling to room temperature the electrodes were soaked in 1 M NaOH solution for 30 min to remove the excess V_2O_5 present in the $BiVO_4$ films. The obtained pure $BiVO_4$ electrodes were rinsed with deionized water and dried in ambient air.

The obtained $BiVO_4$ photoanodes were used directly without doping with other elements. The undoped $BiVO_4$ serves as an excellent starting material to demonstrate

the advantage of forming p-n heterojunction with cocatalysts. This simplified model electrode could facilitate the isolation of determining factors in the charge separation process in p-n junctions.

Preparation of Co_3O_4 nanoparticles

The Co_3O_4 nanoparticles were synthesized by a facile hydrothermal method. In a typical procedure, 0.4 mL ammonium solution ($NH_3 \cdot H_2O$, 25 wt%) was added into 25 mL 1 mM cobalt acetate aqueous solution, followed by stirring for 15 min. Then the solution was transferred to a 50 mL Teflon-lined stainless steel autoclave. The hydrothermal synthesis was conducted at 150 ºC for 3 h. After the stainless autoclave was cooled to room temperature by flowing water, the obtained products were centrifuged, washed with deionized water and ethanol for three times, respectively. Lastly, the obtained samples were dried in 80 ºC for several hours in a drying oven.

The smaller Co_3O_4 nanoparticles (~4 nm) were synthesized by the similar method mentioned above. In a typical procedure, 0.4 mL ammonium solution ($NH_3 \cdot H_2O$, 25 wt%) was added into 25 mL 1 mM cobalt acetate ethanol solution, followed by stirring for 15 min. Then the solution was transferred to a 50 mL Teflon-lined stainless steel autoclave. The hydrothermal synthesis was conducted at 120 ºC for 1 h. The obtained products were centrifuged, washed and dried by the same way mentioned above.

Preparation of $Co_3O_4/BiVO_4$ composites

A drop-casting technique was used to synthesize the $Co_3O_4/BiVO_4$ composites. Firstly, 20 mg of Co_3O_4 nanoparticles were dispersed in 100 mL absolute ethanol and sonicated for 30 min to form a uniform nanoparticle "ink". The "ink" was then drop-casted onto the $BiVO_4$ electrodes. The drop-casted area was controlled to be 1 cm^2 and the mass of Co_3O_4 was adjusted by the drop volume of "ink". The composites were fully dried at 80 ºC for 30 min and then annealed at 450 ºC (ramping rate = 1 ºC/min) for 2 h.

Before applying the "ink", the mass of $BiVO_4$ film in 1 cm^2 was determined to be 0.5 ± 0.04 mg by scraping the films off from FTO substrates using 10 dummy samples prepared in the same batch with those used for further measurements. The Co_3O_4 concentration of the "ink" was known. Therefore, the loading weight of Co_3O_4 could be accurate controlled by adjusting the drop volume of "ink". In order to investigate the effects of Co_3O_4 loading on the photocatalytic activity, the $Co_3O_4/BiVO_4$ composites with various Co_3O_4 loading weight (2.0, 4.0, and 8.0 wt%) were prepared.

Physical Characterization

The morphology and microstructure of the samples were characterized by field-emission scanning electron microscopy (FESEM) (Hitachi S-4800, 5 kV) with energy-dispersive X-ray spectrum (EDX). Transmission electron microscopy (TEM), high-resolution TEM (HRTEM) images were obtained on a JEOL JEM-2100F microscope

at 200 kV. Prior to the measurements, the $Co_3O_4/BiVO_4$ composites were detached from the FTO substrate and ultrasonically dispersed in ethanol, and dipped onto a copper grid with a lacey carbon film and dried under ambient conditions. The crystal structure was determined by X-ray diffractometer (D/MAX-2500) with Cu Kα radiation (λ = 1.5416 Å) at 40 kV and 140 mA. XRD spectra were collected over a 2θ range of 10-90º at a scanning speed of 0.02º per step. The optical absorptance of as-prepared samples were obtained using a Shimadzu UV-2550 spectrophotometer equipped with an integrating sphere using $BaSO_4$ as the reflectance standard. The photoluminescence (PL) spectra were obtained using a Hitachi fluorescence spectrophotometer with excitation of 350 nm wavelength incident-light at ambient temperature.

Photoelectrochemical measurements

Photoelectrochemical performances of as-prepared $BiVO_4$ and $Co_3O_4/BiVO_4$ electrodes were all achieved with front-side illumination and evaluated using a three-electrode configuration, with the nanoporous photoanodes ($BiVO_4$ or $Co_3O_4/BiVO_4$ electrodes) as the working electrode, a platinum foil (2 × 2 cm^2) as the counter electrode, and saturated Ag/AgCl as the reference electrode. The simulated solar illumination was obtained by passing light from a 300 W Xenon arc lamp (Beijing Perfectlight Technology Co. Ltd., Microsolar 300 UV) equipped with an AM 1.5 filter, and the power intensity of the incident light was calibrated to 100 mW/cm^2 at the surface of the working electrode. All illuminated areas were 1 cm^2. An electrochemical workstation (IVIUM CompactStat.e20250) was used to measure the current-voltage (*J-V*) characteristic of the electrodes, with a scan rate of 50 mV/s. A 0.5 M potassium phosphate (KH_2PO_4) buffer solution (PH 7) with or without 1 M sodium sulfite (Na_2SO_3) as a hole scavenger was used as the electrolyte. Prior to measurements, the electrolyte was thoroughly deaerated by purging it with N_2 for 0.5 h. Chopped-light amperometric *J-t* characterizations were evaluated at an applied potential of 0.6 V *vs.* RHE under chopped light irradiation (light on or off cycles: 10 s). The incident photo to current efficiency (IPCE) was measured at 1.23 V *vs.* RHE for the $BiVO_4$ and $Co_3O_4/BiVO_4$ electrodes in the electrolyte mentioned above under AM 1.5G irradiation. Electrochemical impedance spectroscopy (EIS) was conducted by applying an AC voltage amplitude of 50 mV within the frequency range from 10^5 to 10^{-3} Hz in 0.5 M KH_2PO_4 buffer solution with or without 1 M Na_2SO_3 under the open-circuit potential (OCP) and AM 1.5G illumination (100 mW/cm^2). The Mott-Schottky plots were measured in a 0.5 M KPi buffer (pH 7) at a frequency of 1000 Hz and amplitude of 10 mV under the dark condition. The measured potentials *vs.* Ag/AgCl were converted to the reversible hydrogen electrode (RHE) scale according to the Nernst equation: $E_{RHE} = E_{Ag/AgCl} + 0.059 \times pH + 0.1976$.

Supplemental Figures and Tables

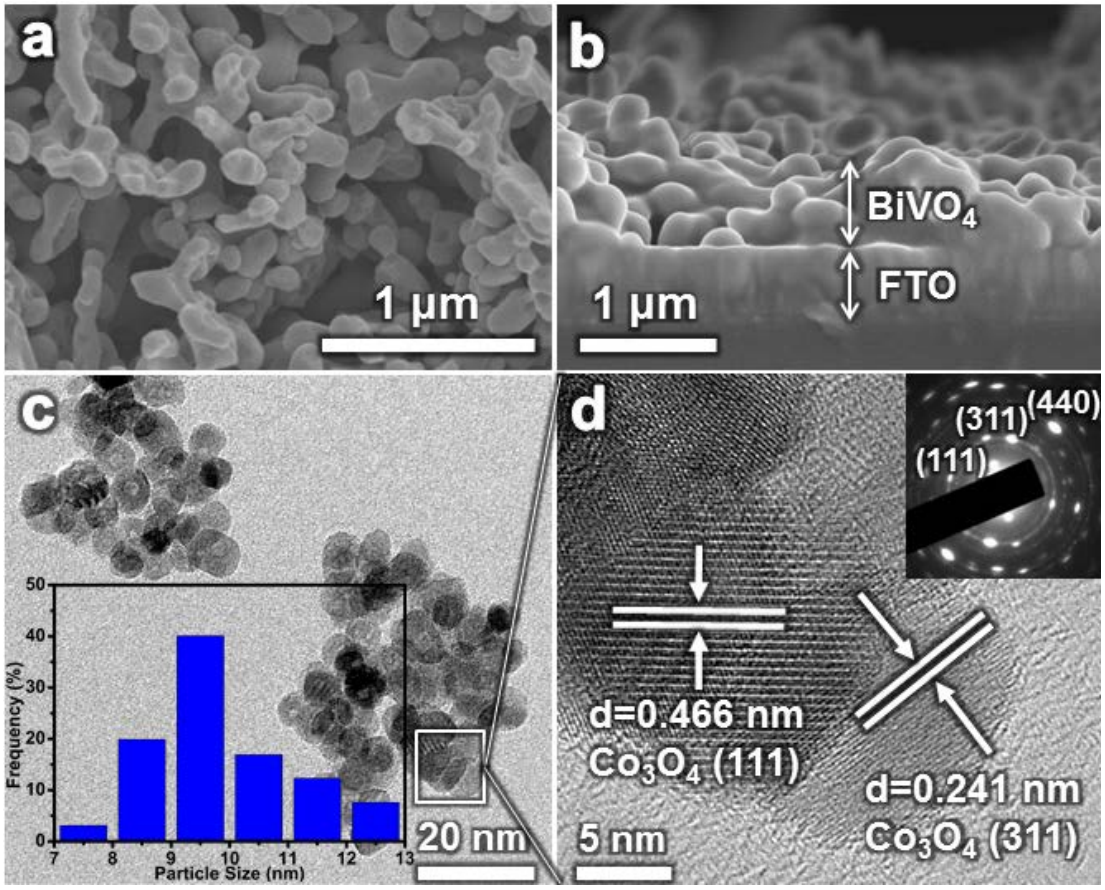

Figure S1. (a) Top-view and (b) side-view FESEM images of pure $BiVO_4$ films; The thickness of $BiVO_4$ film is 700 ± 50 nm on average based on the side-view FESEM images of 10 locations. (c) Transmission electron microscopy (TEM) image (the particle size distribution shown as inset) and (d) high-resolution TEM (HRTEM) image of Co_3O_4 nanoparticles.

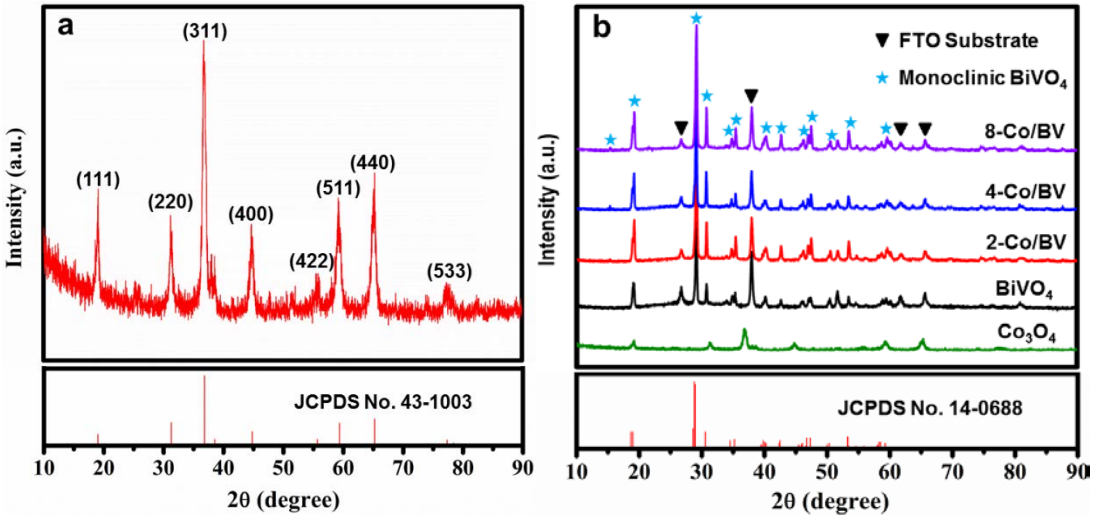

Figure S2. XRD patterns of (a) Co_3O_4 and (b) $Co_3O_4/BiVO_4$ composites with different loading amount. The peaks marked with asterisk and triangle originate from monoclinic $BiVO_4$ and FTO substrate respectively. Vertical bars indicate peak position and intensity of Co_3O_4 and monoclinic $BiVO_4$ (JCPDS No. 43-1003 and 14-0688). The absence of the strongest characteristic peak of Co_3O_4 at 37° on the $Co_3O_4/BiVO_4$ composites line pattern in Figure S2b indicates the high dispersion of Co_3O_4.

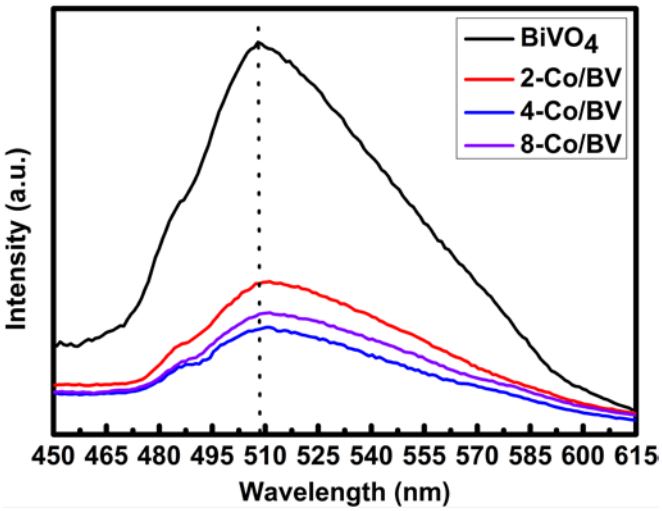

Figure S3. PL spectra of different samples at room temperature.

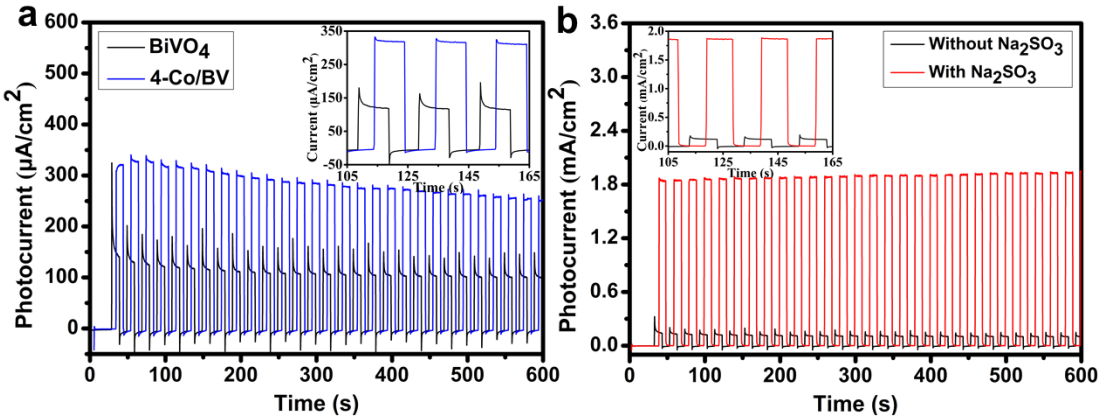

Figure S4. Photocurrent transients of (a) $BiVO_4$ and 4-Co/BV in phosphate buffer solution (pH 7); (b) pure $BiVO_4$ in phosphate buffer solution with and without Na_2SO_3 measured at 0.6 V *vs.* RHE under AM 1.5G illumination (100 mW/cm^2). The insets are expanded views of the photocurrent transients.

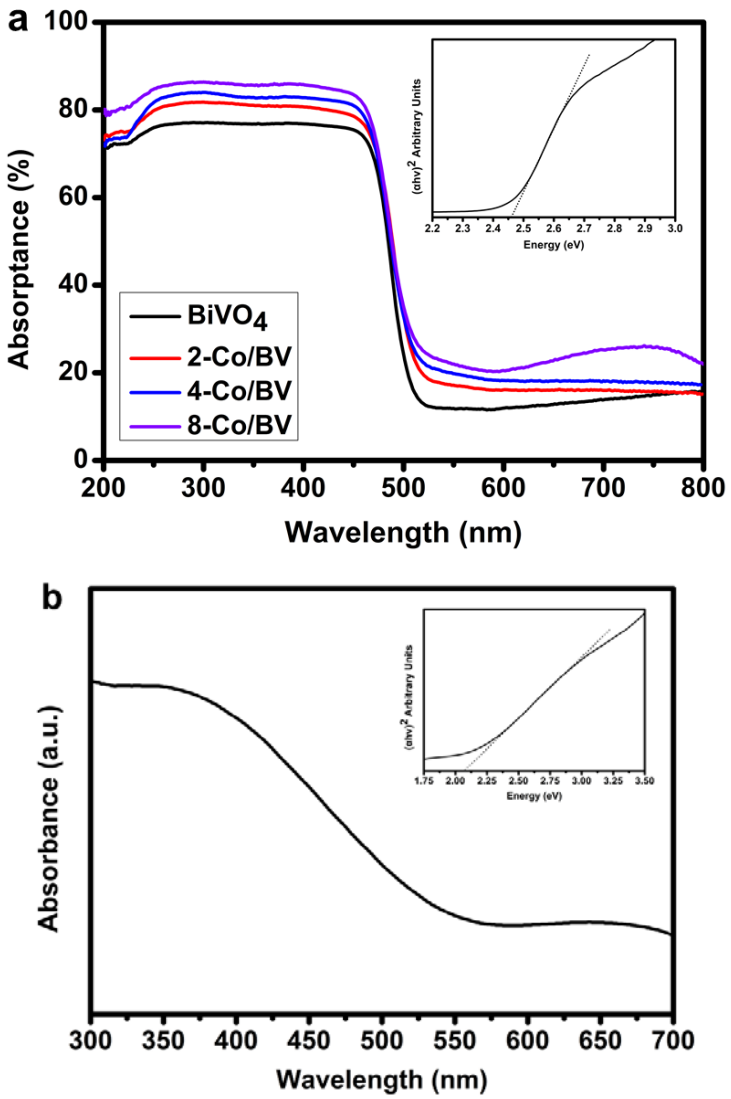

Figure S5. (a) UV-visible absorptance spectra of different samples and the Tauc plots of $BiVO_4$ shown inset; (b) UV-visible absorbance spectra of pure Co_3O_4 and the Tauc plots of Co_3O_4 shown inset.

Table S1. The absolute electronegativity, band gap energy, energy levels of calculated conduction band edge and valence band edge at the point of zero charge and pH 7 for Co_3O_4 and $BiVO_4$.

Semiconductor	Absolute electronegativity (X)	Band gap energy (eV)	Conduction band edge (V *vs.* NHE)		Valence band edge (V *vs.* NHE)	
			pH_{zpc}	pH 7	pH_{zpc}	pH 7
$BiVO_4$	6.035	2.46	0.31	0.08	2.77	2.54
Co_3O_4	5.903	2.07	0.37	0.35	2.44	2.42

The absolute electronegativity (X) of $BiVO_4$ and Co_3O_4 can be estimated to be 6.035 and 5.903 from the references.[3,4] The band gap energy (E_g) can be estimated from the Tauc plots shown in the insets of Figure S5. The valence band edge of a semiconductor at the point of zero charge (pH_{zpc}) can be estimated by equation 1 as follows:

$$E_{VB}^0 = X - 4.5 + E_g/2 \quad (1)$$

where 4.5 is the energy of free electrons on the hydrogen scale. Meanwhile, the points of zero charge of $BiVO_4$ and Co_3O_4 are 3 and 7, respectively.[4] Therefore, the calculated valence band edge at the point of zero charge can be corrected to pH 7 by the following methods:

$$E_{VB}^0 + (pH_{zpc} - 7) \times 0.059$$

Then, the conduction band edge can be calculated by equation 2 as follows:

$$E_{CB} = E_{VB} + E_g \quad (2)$$

The photocurrent density arising from PEC performance (J_{PEC}) can be described as follows:

$$J_{PEC} = J_{abs} \times \eta_{bulk} \times \eta_{surface} \quad (3)$$

where J_{abs} is the photocurrent density when completely converting the absorbed photons into current (i.e., APCE = 100%). Adding 1 M Na_2SO_3 to the electrolyte can completely suppress the surface recombination of charge carriers without influencing the charge separation in the electrode bulk (i.e., $\eta_{surface}$ = 100%). Therefore, η_{bulk} and $\eta_{surface}$ can be determined as follows:

$$\eta_{bulk} = J_{sulfite} / J_{abs} \quad (4)$$

$$\eta_{surface} = J_{water} / J_{sulfite} \quad (5)$$

where J_{water} and $J_{sulfite}$ is the photocurrent density for PEC water oxidation and sulfite oxidation, respectively. By estimating the overlapped areas between the UV-vis absorptance spectrum (Figure S5) and the AM 1.5G solar spectrum, assuming APCE = 100%, the J_{abs} of $BiVO_4$ was calculated to be 5.2 mA/cm^2. This value is slightly higher than the reported ones[5,6] because of some other factors including surface morphology and the consequently slight enhancement in light absorption. With the loading of Co_3O_4,

the ability of light absorption was enhanced, which resulted in the J_{abs} of 6.7, 6.9 and 7.2 mA/cm^2 for 2-Co/BV, 4-Co/BV and 8-Co/BV, respectively. Therefore, the efficiency of charge separation in the bulk and on the surface of the photoelectrodes can be determined independently using the equation 3-5, as displayed in Figure 3.

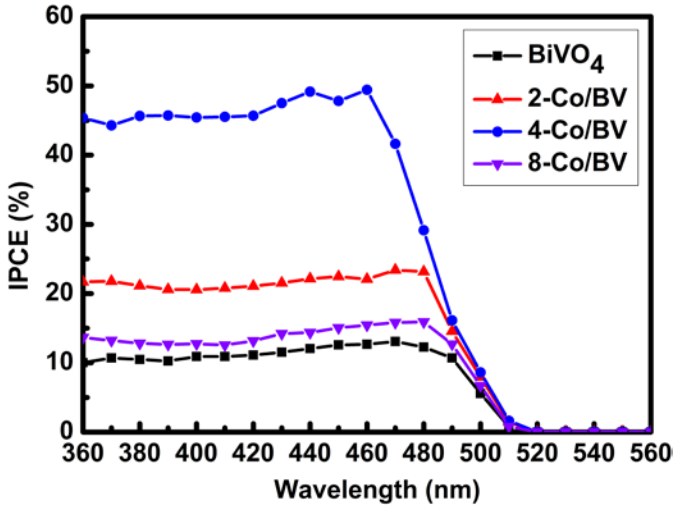

Figure S6. The incident photon-to-electron conversion efficiency (IPCE) spectra of $BiVO_4$, 2-Co/BV, 4-Co/BV and 8-Co/BV in phosphate buffer solution (pH 7) measured at 1.23 V *vs.* RHE with front illumination.

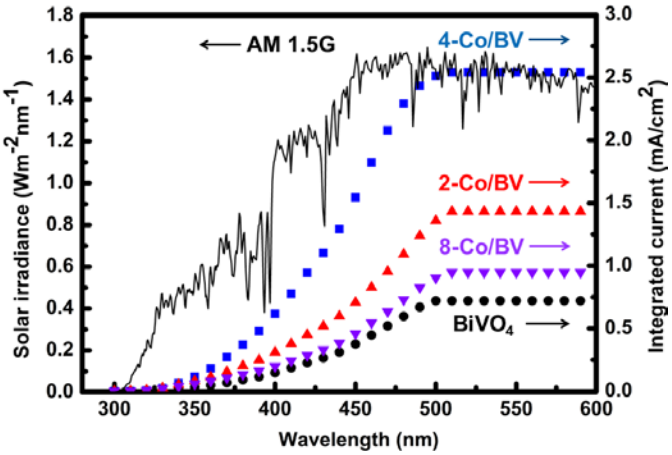

Figure S7. Solar irradiance of AM 1.5G (ASTM G173-03) and calculated photocurrent of $BiVO_4$, 2-Co/BV, 4-Co/BV and 8-Co/BV by integrating IPCE over the photon flux of AM 1.5G. In addition to bare $BiVO_4$ and 4-Co/BV mentioned in the main text, the estimated photocurrent density of ~1.44 mA/cm^2 for 2-Co/BV and ~0.95 mA/cm^2 for 8-Co/BV were very close to the measured values of 1.52 mA/cm^2 and 1.003 mA/cm^2 for 2-Co/BV and 8-Co/BV at 1.23 V *vs.* RHE in the *J-V* curves, respectively. This indicates that the measured *J-V* curves using our solar simulator are in consistence with the IPCE data measured by our monochrometer.

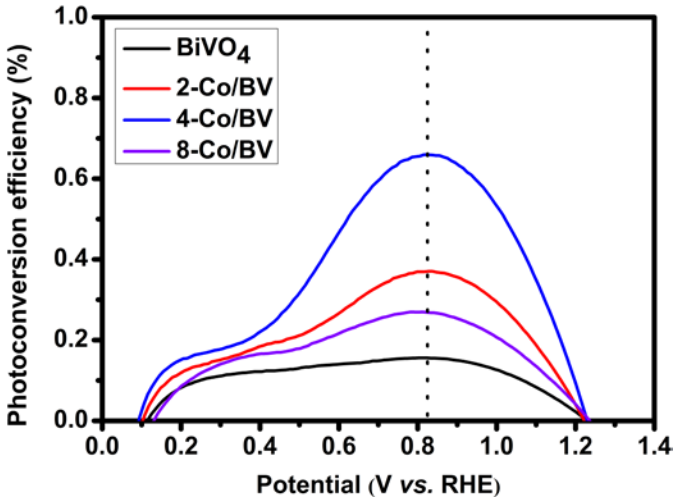

Figure S8. Photoconversion efficiencies for pure $BiVO_4$, 2-Co/BV, 4-Co/BV and 8-Co/BV as a function of applied potential *vs.* RHE measured in phosphate buffer solution (pH 7).

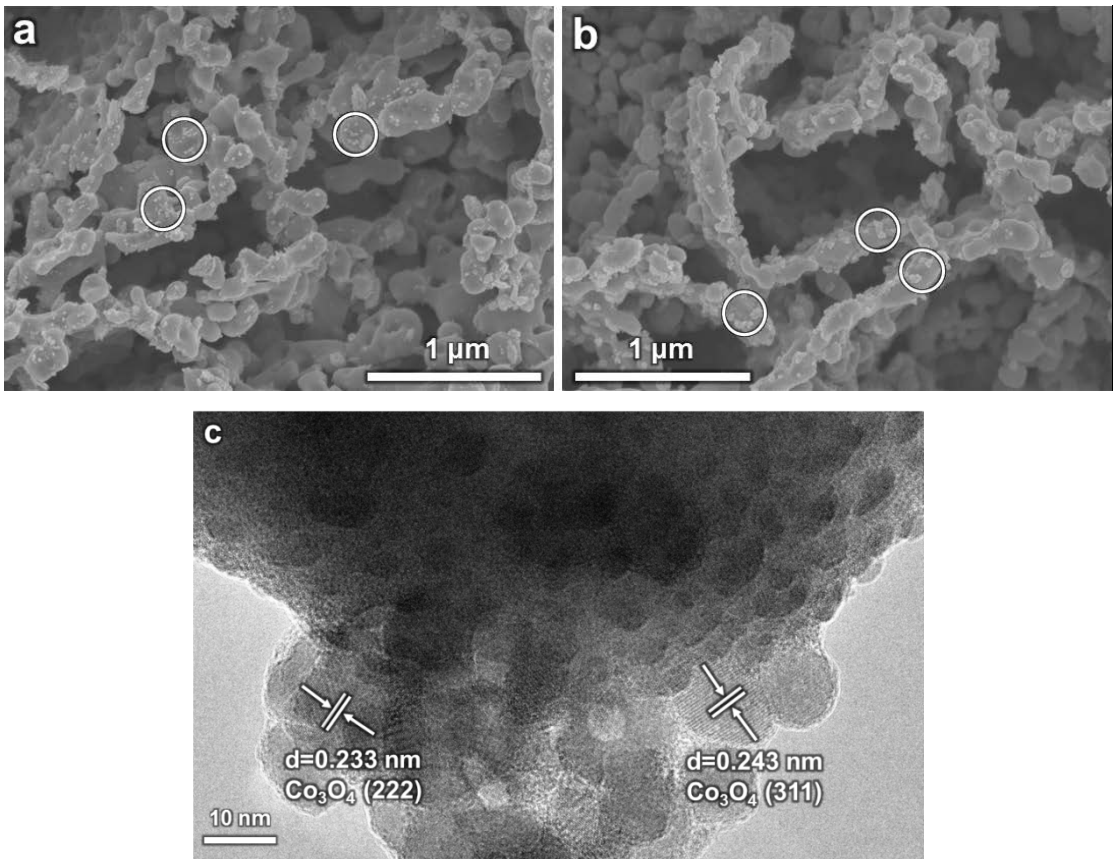

Figure S9. FESEM images of (a) 4-Co/BV and (b) 8-Co/BV; (c) TEM image of 8-Co/BV.

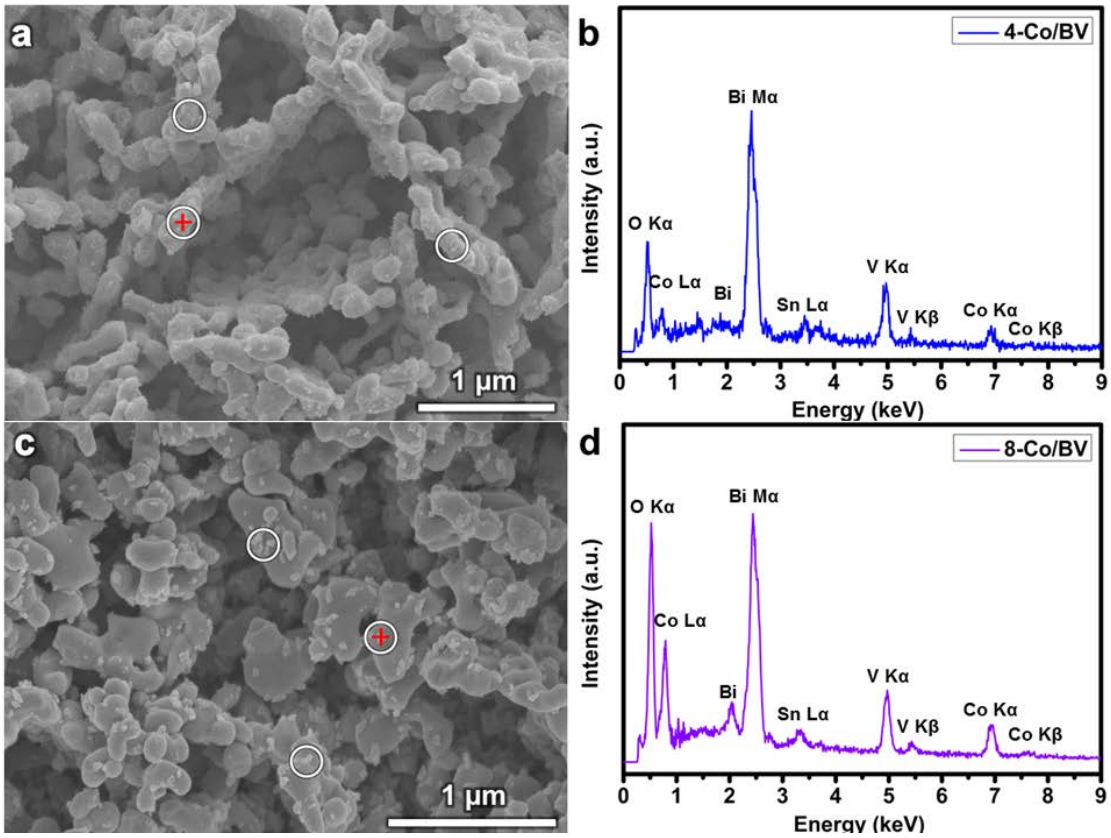

Figure S10. FESEM images of (a) 4-Co/BV and (c) 8-Co/BV; EDX data of (b) 4-Co/BV and (d) 8-Co/BV.

In order to confirm the particles and clusters within the white circles of Figure 1b, S9a and b were Co_3O_4, EDX analysis was conducted for 4-Co/BV and 8-Co/BV at the locations marked by red crosses in FESEM images (Figure S10a, c). The presence of the characteristic EDX cobalt peaks for both 4-Co/BV and 8-Co/BV (Figure S10b, d) confirms the assignment of Co_3O_4. The peak of tin was resulted from F:SnO_2 on the FTO substrates.

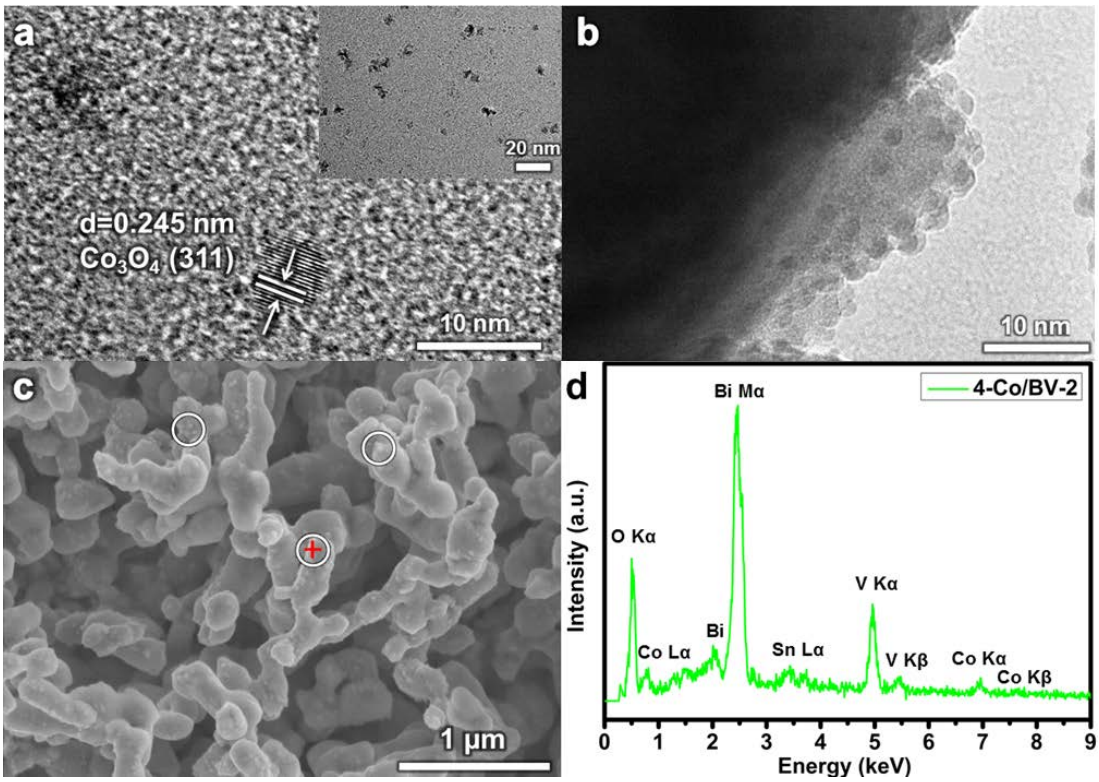

Figure S11. (a) TEM and HRTEM images of smaller 4 nm Co_3O_4 nanoparticles; (b) TEM image and (c) FESEM image of 4-Co/BV-2; (d) EDX data of 4-Co/BV-2.

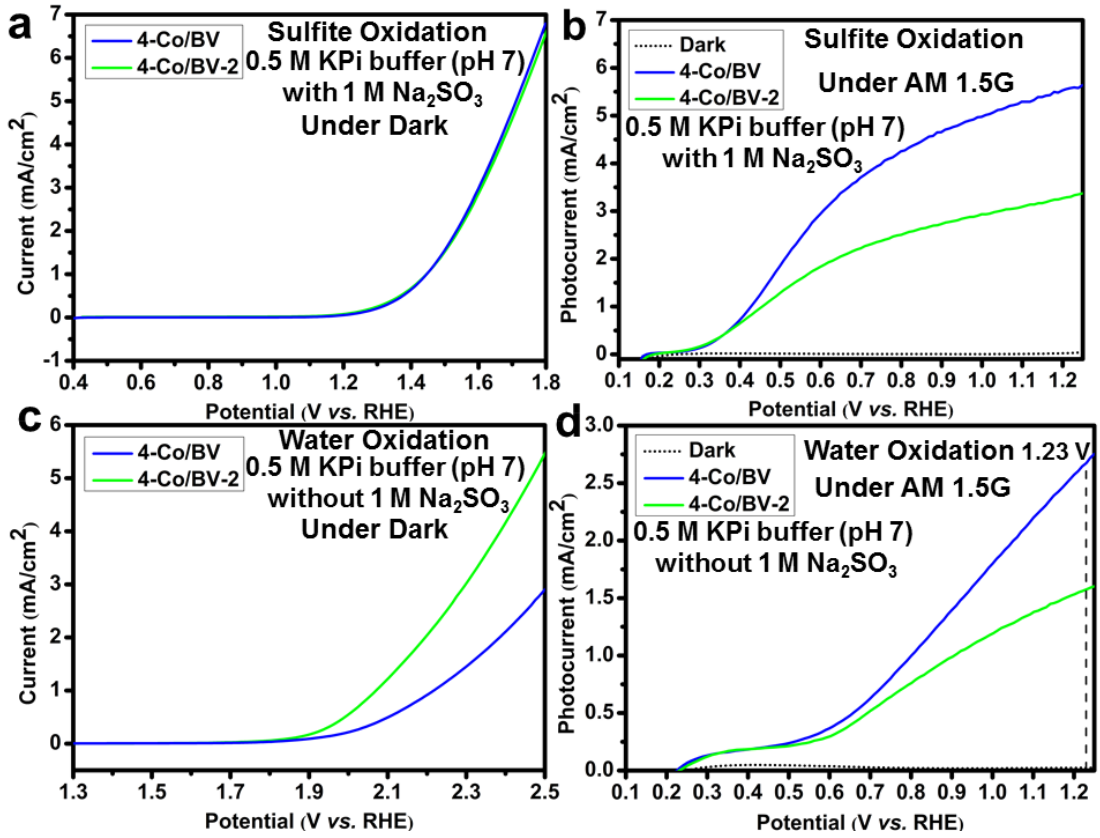

Figure S12. *J-V* curves of 4-Co/BV and 4-Co/BV-2 measured (a, c) without and (b, d) with AM 1.5G illumination (100 mW/cm^2) for (a, b) sulfite oxidation (with 1 M Na_2SO_3) and (c, d) water oxidation (without 1 M Na_2SO_3).

The aggregation of cocatalyst particles is expected to reduce the catalytic performance due to the introduction of inter-particle interfaces. On the other hand, smaller cocatalyst particles may improve the catalytic performance owing to the increase of surface area. Considering the mutually weakening relationship between aggregation and particle size, a carefully controlled comparison may provide future insights into the effect of particle aggregation on the overall catalytic performance.

Smaller Co_3O_4 particles with an average diameter of ~4 nm (Figure S11a) were synthesized and loaded onto $BiVO_4$ with 4.0 wt% (denoted as 4-Co/BV-2) for comparison with 4-Co/BV (~10 nm Co_3O_4 particles). These ~4 nm particles were confirmed to be Co_3O_4 using EDX (Figure S11c and d). As expected, smaller Co_3O_4 particles with higher surface energy are more likely to aggregate than the large ones, as illustrated by huge Co_3O_4 cluster composed of ~4 nm particles (Figure S11b) and the highly dispersed ~10 nm Co_3O_4 particles (Figure 1c).

The PEC performance of 4-Co/BV and 4-Co/BV-2 were acquired with front-side illumination and shown in Figure S12. For the fast sulfite oxidation, 4-Co/BV and 4-Co/BV-2 exhibit similar *J-V* behavior in the dark (Figure S12a), suggesting the equally fast sulfite oxidation kinetics on both samples, independent of the degree of aggregation. However, the aggregation of Co_3O_4 particles on 4-Co/BV-2 may exhibit more interfacial defects and larger resistance for charge carriers. Therefore, the PEC performance of 4-Co/BV-2 for sulfite oxidation under AM 1.5G illumination was reduced compared to 4-Co/BV (Figure S12b). For the relatively sluggish water oxidation, 4-Co/BV-2 shows a catholic shift of onset potential compared to 4-Co/BV in the dark (Figure S12c), indicating the improved surface catalytic effect of 4-Co/BV-2 owing to the intrinsic high surface-to-volume ratio of smaller ~4 nm particles. However, the improved surface catalytic effect of smaller particles is unable to outperform the adverse effect of particle aggregation under under AM 1.5G (Figure S12d). Upon illumination, the number of available photogenerated charge carriers becomes a rate limiting factor, which is sensitive to the recombination at inter-particle interfaces. Therefore, for the $BiVO_4/Co_3O_4$ photoande/cocatalyst system, the adverse effect of particle aggregation is more prominent than the higher surface area obtained by reducing the Co_3O_4 size form 10 nm to 4 nm. The aggregation of Co_3O_4 particles should be avoided.

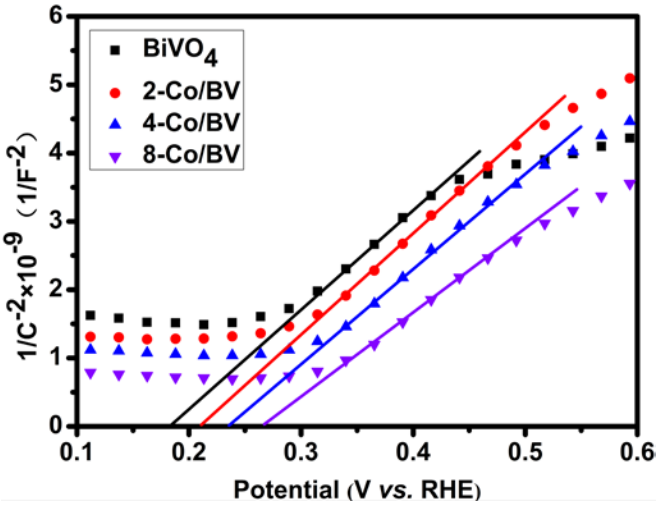

Figure S13. Mott-Schottky plots of $BiVO_4$, 2-Co/BV, 4-Co/BV and 8-Co/BV measured in a 0.5 M KPi buffer (pH 7) in dark (1 kHz).

The Mott-Schottky plots of $BiVO_4$, 2-Co/BV, 4-Co/BV and 8-Co/BV are shown in Figure S13 to investigate the shifts in the effective flat-band position. Although it is difficult to determine the exact flat-band potential (E_{FB}) of these samples since the Mott-Schottky equation was based on a planar electrode, the effective E_{FB} can provide qualitative insights into the formation of p-n junctions.[7,8]

Compared with the bare $BiVO_4$ sample, all the three Co_3O_4 loaded samples exhibit positive shifts of effective E_{FB}, indicating the formation of p-n heterojunction between Co_3O_4 and $BiVO_4$ because of the p-type characteristic of Co_3O_4 and its high point of zero ζ potential (pH_{PZZP}), which will shift the E_{FB} positively.[1]

Moreover, the slopes of Mott-Schottky plots of Co_3O_4 loaded $BiVO_4$ photoanodes are comparable with that of bare $BiVO_4$ photoanodes. This suggests that the loading of Co_3O_4 nanoparticles did not affect the charge carrier density within the $BiVO_4$ electrodes.

Table S2a. Fitting results and the accuracy of R_Ω for different samples in phosphate buffer solution without Na_2SO_3 by ZVIEW.

	$BiVO_4$	**2-Co/BV**	**4-Co/BV**	**8-Co/BV**
***R_Ω* (Ω)**	31.30	32.82	34.60	47.50
Error (%)	1.59	2.36	0.89	0.77

Table S2b. Fitting results and the accuracy of R_Ω for different samples in phosphate buffer solution with Na_2SO_3 by ZVIEW.

	$BiVO_4$	**2-Co/BV**	**4-Co/BV**	**8-Co/BV**
***R_Ω* (Ω)**	23.90	25.60	26.69	39.90
Error (%)	2.03	1.00	1.94	2.05

References

(1) Kim, T. W.; Choi, K. S. *Science* **2014**, *343*, 990.

(2) McDonald, K. J.; Choi, K. S. *Energy Environ. Sci.* **2012**, *5*, 8553.

(3) Long, M.; Cai, W.; Cai, J.; Zhou, B.; Chai, X.; Wu, Y. *J. Phys. Chem. B* **2006**, *110*, 20211.

(4) Wang, J. R.; Osterloh, F. E. *J. Mater. Chem. A* **2014**, *2*, 9405.

(5) Zhou, M.; Bao, J.; Bi, W.; Zeng, Y.; Zhu, R.; Tao, M.; Xie, Y. *ChemSusChem* **2012**, *5*, 1420.

(6) Jeong, H. W.; Jeon, T. H.; Jang, J. S.; Choi, W.; Park, H. *J. Phys. Chem. C* **2013**, *117*, 9104.

(7) Klahr, B.; Gimenez, S.; Santiago, F. F.; Bisquert, J.; Hamann, T. W. *Energy Environ. Sci*., **2012**, *5*, 7626.

(8) Cardon, F.; Gomes, W. P. *J. Phys. D: Appl. Phys.*, **1978**, *11*, 63.